

N76-10180

LARGE ANGLE SATELLITE ATTITUDE MANEUVERS

John E. Cochran* and **John L. Junkins†**
The University of Virginia
Charlottesville, Virginia

ABSTRACT

Two methods are proposed for performing large angle reorientation maneuvers. The first method is based upon Euler's Rotation Theorem; an arbitrary reorientation is ideally accomplished by rotating the spacecraft about a line (the "Euler Axis" or "Principal Line") which is fixed in both the body and in space. This scheme has been found to be best suited for the case in which the initial and desired attitude states have small angular velocities. A detailed evaluation of the associated feedback control laws and sensitivity to disturbances has been carried out, assuming the control system to consist of four single-gimbal control moment gyros (CMGs). These results indicate that the proposed scheme is feasible with realistic physical constraints on the CMG torque source. The second scheme is more general in that a general class of transition trajectories is introduced which, in principle, allows transfer between arbitrary orientation and angular velocity states. The method generates transition maneuvers in which the uncontrolled (free) initial and final states are matched in orientation and angular velocity. The forced transition trajectory is obtained by using a weighted average of the unforced forward integration of the initial state and the unforced backward integration of the desired state.

Our current effort is centered around practical validation of this second class of maneuvers. Of particular concern is enforcement of given control system constraints and methods for suboptimization by proper selection of maneuver initiation and termination times. Analogous reorientation strategies which force smooth transition in angular momentum and/or rotational energy are also under consideration.

DISCUSSION

Many spacecraft must perform one or more reorientations or attitude changes during their lifetimes. The ways in which these maneuvers are performed are obviously important from the standpoint of conservation of energy. However, often the optimality of a maneuver in

*Visiting Associate Professor, Associate Professor, Aerospace Engineering Department, Auburn University, Auburn, Alabama.
†Associate Professor.

terms of the energy required to perform it may be of lesser importance than the time and computational power needed to define it. That is, often, finding the optimal maneuver strategy may not be desirable or even possible within the constraints imposed.

In this paper, two methods for defining "good," nominal, large-angle attitude maneuvers for spacecraft are presented. Neither of the methods is generally optimal (although in special cases they would be), but both offer the advantages of being (1) relatively easy to use and (2) explicit, rather than iterative. The first method, which is well-suited for the case of quiescent initial and final rotational states, is based on Euler's Rotation Theorem, that is, it is a single axis maneuver. The second method, which may be used when the initial and/or final rotational states are not quiescent, is based on the use of transition trajectories in a phase space of dimension eight, where the redundant dimensions are due to the choice of four parameter descriptions of orientation.

SINGLE AXIS MANEUVERS

The idea of utilizing single axis rotations for arbitrary reorientations is not a new idea (Meyer, 1966). For example, the Apollo Command and Service Module were reoriented with a single rotation about the required Euler axis (Crisp et al., 1967). Such maneuvers are not necessarily optimal, in fact, Dixon et al. (1970) have shown that single axis maneuvers of axisymmetric spacecraft through the use of thrusters are generally more costly in terms of fuel used than two-impulse maneuvers designed to minimize fuel expended. They are, on the other hand, more easy to define than optimal maneuvers, and if the spacecraft is asymmetric, no closed-form optimal maneuver strategy comparable to that of Dixon et al. (1970) is available.

One important concept, used to some extent in both methods, is that of Euler, or eigenaxis, rotations. Figure 1 is included to illustrate this concept. On the left hand side of figure 1 are shown a centroidal body-fixed system $Cxyz$ and the associated unit vector triad ($\hat{u}_1, \hat{u}_2, \hat{u}_3$) as well as the Euler axis for a particular reorientation. The $Cxyz$ system pictured on the right-hand side is a rotationally inertial coordinate system which is used along with the displaced $Cxyz$ system to indicate how the Euler axis rotation proceeds.

Figure 2 provides some information concerning how the attitude of a moving trihedral $C \hat{e}_1 \hat{e}_2 \hat{e}_3$ with respect to a fixed trihedral $C \hat{e}'_1 \hat{e}'_2 \hat{e}'_3$ can be defined. The rotation matrix $\underline{\Delta}$, whose elements are direction cosines relating the two trihedrals, can be constructed using Euler angles, say ψ, θ , and ϕ or alternatively using Euler parameters, here indicated by $\alpha_0, \alpha_1, \alpha_2$, and α_3 . Furthermore, the Euler parameters are intimately related to the principal rotation angle ϕ and the direction cosines ℓ_1, ℓ_2 , and ℓ_3 of the principal line, i.e., the Euler axis (or equivalently, the eigenaxis corresponding to the unit eigenvalue of $\underline{\Delta}$).

Assuming that $\underline{\Delta}$ is specified, the four parameters $\alpha_0, \alpha_1, \alpha_2$, and α_3 can be determined in a noniterative fashion. Then, for single axis rotations, the direction of the Euler axis can be determined as well as the required principal angle. For control of single axis rotations in the presence of disturbing torques, it is advantageous to define an eigenaxis system as

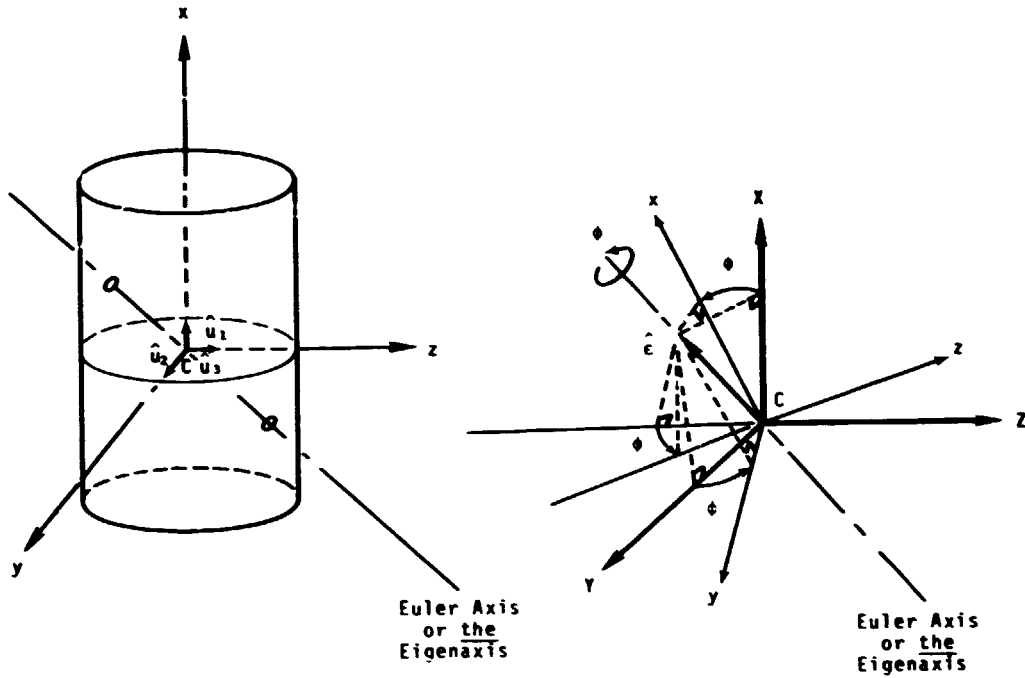


Figure 1. The Euler axis and Euler axis rotations.

$$[\hat{e}_1, \hat{e}_2, \hat{e}_3]^T = A[\hat{e}_1, \hat{e}_2, \hat{e}_3]^T$$

$$A = A(\psi, \theta, \phi) = A(\alpha_0, \alpha_1, \alpha_2, \alpha_3)$$

$$\alpha_0 = \cos(\phi/2) \quad \alpha = \sum_{j=1}^3 \underbrace{([\sin(\phi/2)] \hat{e} \cdot \hat{e}_j)}_{\alpha_j} \hat{e}_j$$

$$Q = \alpha_0 + \underline{\alpha} \quad Q^{-1} = \alpha_0 - \underline{\alpha}$$

$$\hat{e}_j = Q \hat{e}_j^0 Q^{-1} \quad \alpha_j = \hat{e} \cdot \hat{e}_j^0, \quad j = 1, 2, 3.$$

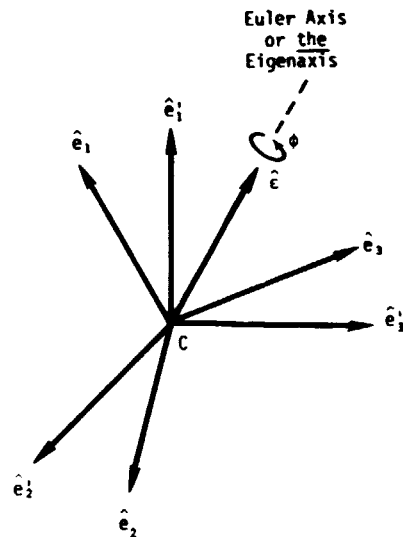


Figure 2. Attitude change logic.

described in Cochran et al., 1975. The way in which such a system is defined is briefly summarized in figure 3.

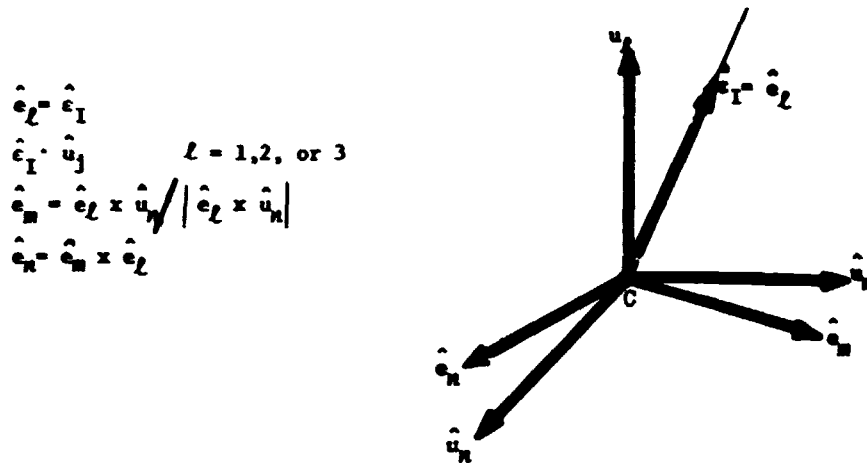


Figure 3. The eigenaxis system.

Figure 4 indicates how attitude errors in the form of small Euler angles ϕ_m and ϕ_n may be specified by using the body-fixed eigenaxis system $Ce_l e_m e_n$ which ideally has its \hat{e}_l -axis directed along the principal line.

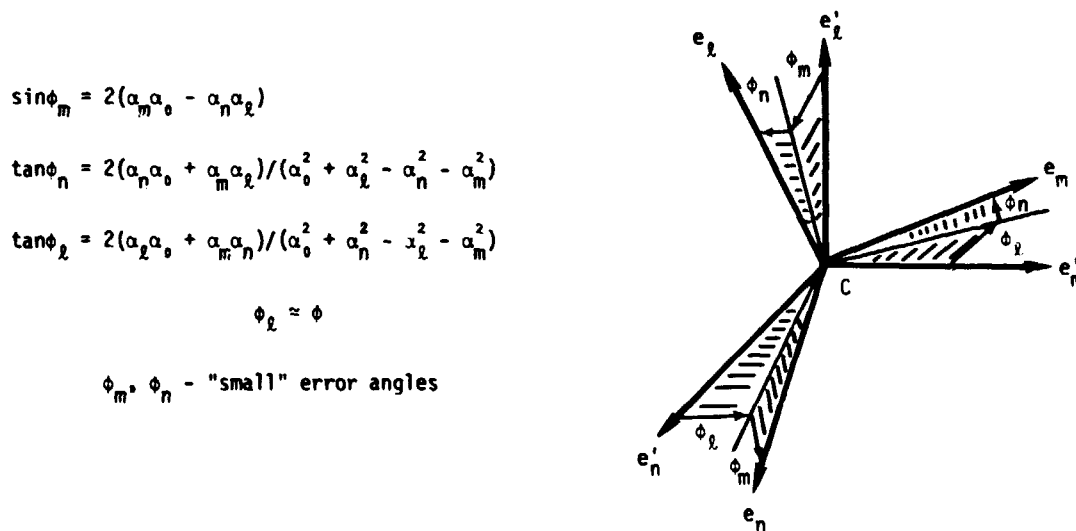


Figure 4. Attitude errors.

The dynamical equations for a spacecraft which contains n control moment gyros (CMGs) are given in figure 5. This equation, the control torque equation, and CMG steering law also given in figure 5 were used in a recent study (Cochran et al., 1975) of the feasibility of controlling single axis rotations using CMGs and several linear controllers.

$$\text{Dynamics: } \underline{I} \underline{\dot{\Omega}} + \tilde{\underline{\Omega}} \underline{I} \underline{\Omega} = \underline{T}_{ex} + \underline{T}_c$$

$$\text{Control torque: } \underline{T}_c = -\underline{F} \underline{\delta} + \tilde{\underline{h}}_c \underline{\Omega}$$

$$\text{CMG Steering Law: } \underline{J} = 1/2 \frac{\underline{\delta}^T \underline{W} \underline{\delta}}{\underline{F} \underline{W}^{-1} \underline{F}^T} \underline{W} \underline{\delta}$$

$$\underline{\delta} = -\underline{W}^T \underline{F}^T (\underline{F} \underline{W}^{-1} \underline{F}^T)^{-1} (\underline{T}_c - \tilde{\underline{h}}_c \underline{\Omega})$$

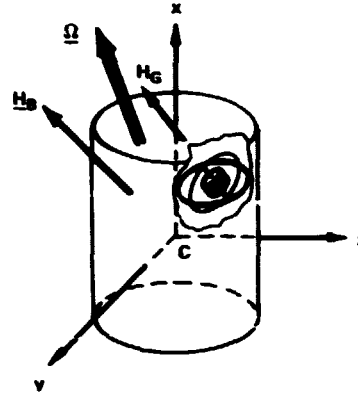


Figure 5. Attitude dynamics and CMG steering law.

The following equations are the nonlinear matrix forms of the equations of rotational motion and approximate linear equations derived assuming small angular velocity magnitude, small errors and a linear controller of angular acceleration (for more details see Cochran et al., 1975).

$$\underline{I}_e \underline{\dot{\Omega}}^e + \tilde{\underline{\Omega}}^e \underline{I}_e \underline{\Omega}^e = \underline{T}_{ex}^e + \underline{T}_c^e$$

$$\underline{\dot{\Omega}}^e = (\ddot{\phi}_1 \ddot{\phi}_2 \ddot{\phi}_3)^T$$

$$\ddot{\phi} = \underline{I}_e^{-1} \underline{T}_{ex}^e + \underline{I}_e^{-1} \underline{T}_c^e$$

$$\ddot{\phi} = \underbrace{-\underline{K}_1 (\dot{\phi} - \dot{\phi}_c) - \underline{K}_2 (\phi - \phi_c) - \underline{K}_3 \int_{t_0}^t (\phi - \phi_c) dt}_{\text{Linear Feedback}}$$

$$+ \underbrace{\underline{I}_e^{-1} \underline{T}_{ex}^e}_{\text{External Disturbance}}$$

One of the controllers used in the study reported in Cochran et al. (1975) is depicted schematically in figure 6. The controller is a proportional-plus-integral-plus-derivative, or PID, controller modified by using a "model follower" commanded rotation angle generator which serves two purposes. First, it allows maintaining the difference in the actual angle of rotation ϕ about the principal line close to the commanded rotation angle ϕ_c (hence higher

gains and tighter control) and second, it provides a means of specifying the nominal rotation rate ω^* a priori so that allowable CMG gimbal rates will hopefully not be exceeded. Attention should be drawn to the form of the function ϕ_c . This function is such that the commanded rotation angle connects the initial value for ϕ , i.e., zero, and the desired final value of ϕ , ϕ_f , with a smooth curve.

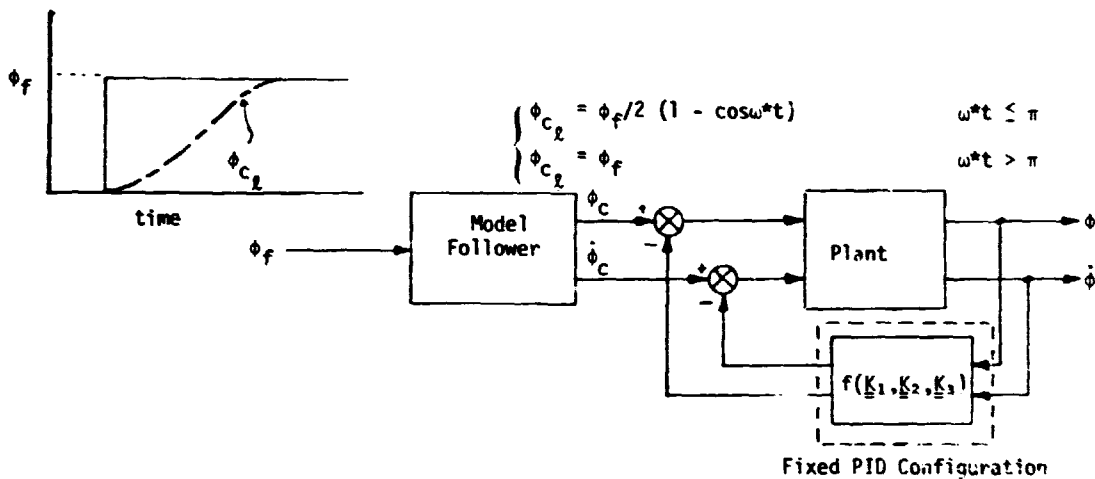


Figure 6. PID model-follower.

Some typical response curves for the rotation angle are shown in figure 7. Four different controllers were used to generate the curves by numerically simulating the attitude motions of a Large Space Telescope type spacecraft using four single gimbal CMGs as torque sources. The full nonlinear equations were used in the simulations (the reader is again referred to Cochran et al. (1975) for more details). The PID model-following controller has been discussed and the PID and PD are simpler controllers. In figure 7, MRAS refers to a model reference adaptive system controller which utilizes Lyapunov's second method to generate variable control gains.

In the study reported by Cochran et al. (1975), the control of single axis rotation in the presence of disturbances was found to be feasible using rate limited CMGs.

TRANSITION TRAJECTORIES

The basic idea for the second method of performing attitude maneuvers was motivated by the use of the function ϕ_c in the PID model-following controller and previous use of the concept of weighting functions in the areas of geodesy and gravity modeling (Jancaitis and Junkins, 1974). In figure 8, this idea, the use of an averaging concept for definition of transition maneuvers, is summarized. The functions $\alpha_f(t)$ and $\alpha_b(t)$, shown in the upper left-hand portion of figure 8, represent an attitude variable, $\alpha(t)$, say one of the α_j , $j = 0, 1, 2, 3$, as it would appear as a function of time if the spacecraft were rotating freely in its initial state (subscript f) and similarly its final, or desired, state (subscript b). The dashed

curve represents a transition curve for the variable α . Note that $\alpha(t)$ is constructed by using the unforced forward integration of α from time t_0 using the actual value of α at t_0 as an initial condition and the unforced backward integration of α from time t_f with the desired final value of α as a final condition.

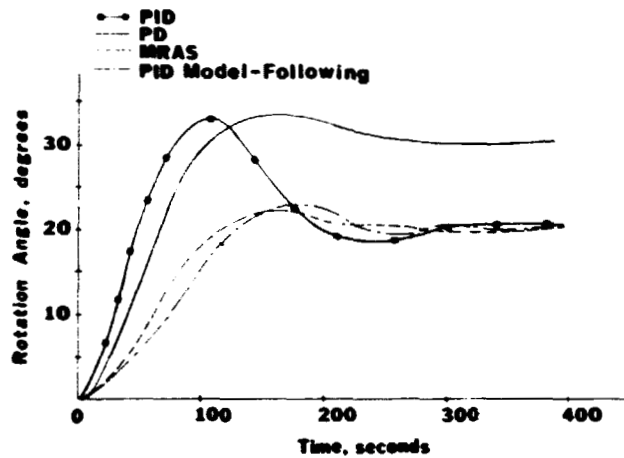
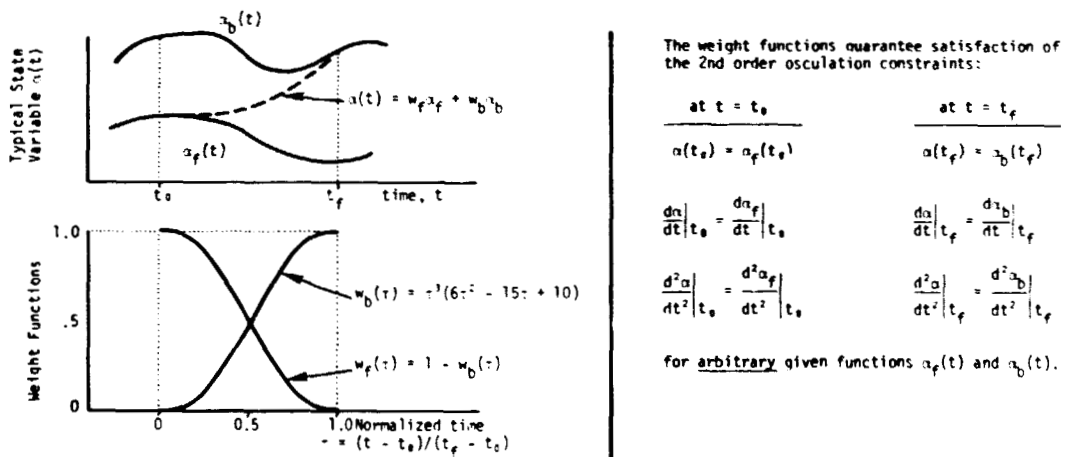


Figure 7. Rotational response.



$\alpha_f(t)$ = Unforced forward integration of actual initial state at time t_0 .

$\alpha_b(t)$ = Unforced backward integration of desired final state at time t_f .

$\alpha(t)$ = "Transition Trajectory" from $\alpha_f(t)$ to $\alpha_b(t) = w_f(\tau)\alpha_f(t) + w_b(\tau)\alpha_b(t)$

Figure 8. Averaging concept for definition of transition maneuvers.

The weighting functions, W_f and W_b , shown as functions of normalized time τ , are used in defining $\alpha(t)$, so that the second-order osculation constraints (see right-hand side of figure 8) of agreement in value and the first two time derivatives at times t_0 and t_f are satisfied. Note that W_f and W_b are relatively simple functions and that they provide a method for defining a smooth function which generates a transition curve between two arbitrary, but smooth, functions of time.

Recalling that α is an attitude variable (it may also be a vector of variables), it is obvious that the proposed method provides a means for explicitly determining the torque required to make the spacecraft attitude follow a prescribed trajectory in phase space. Thus, the trajectory departs smoothly from the initial state and ends in the desired final state. The explicit determination of the torque depends only on the availability of the first two time derivatives of three, or more, attitude variables.

We assume that, during the time required for the maneuvers, the external torques acting on the spacecraft are negligible. Furthermore, in obtaining the results presented here, we have assumed that the spacecraft is a single asymmetric rigid body with known inertia characteristics. These assumptions allow the use of an analytical solution for the free rotational motion of an asymmetric rigid body (see Morton et al., 1973, and Kraige and Junkins, 1974) in computing the forward and backward states and the necessary time derivatives used in constructing the torque required to perform the maneuver.

The analytical solution for the torque-free rotational motion of asymmetric rigid body which was used is summarized in the following list.

Analytical Solution for Torque-Free Motion of Asymmetric Body.

Angular Velocity	Euler Orientation Parameters
$u = \Omega t + \phi_0$ $\omega_1(t) = \omega_{1m} \operatorname{dn}(u, k)$ $\omega_2(t) = \omega_{2m} \operatorname{sn}(u, k)$ $\omega_3(t) = \omega_{3m} \operatorname{cn}(u, k)$	$\{\alpha(t)\} \equiv \begin{Bmatrix} \alpha_0(t) \\ \alpha_1(t) \\ \alpha_2(t) \\ \alpha_3(t) \end{Bmatrix} = \begin{bmatrix} \gamma_0 & -\gamma_1 & -\gamma_2 & -\gamma_3 \\ \gamma_1 & \gamma_0 & -\gamma_3 & \gamma_2 \\ \gamma_2 & \gamma_3 & \gamma_0 & -\gamma_1 \\ \gamma_3 & -\gamma_2 & \gamma_1 & \gamma_0 \end{bmatrix} \begin{Bmatrix} \beta_0(t) \\ \beta_1(t) \\ \beta_2(t) \\ \beta_3(t) \end{Bmatrix}$
<p>where</p> $\{k, \Omega, \phi_0, \omega_{1m}, \omega_{2m}, \omega_{3m}\}$ <p>are constants defined in terms of inertias and initial conditions.</p>	<p>where</p> $\beta_0(t) = \sqrt{\frac{1}{2} [1 + a \operatorname{sn}(u, k)]} \cos \phi_0(t)$ $\beta_1(t) = \sqrt{\frac{1}{2} [1 - a \operatorname{sn}(u, k)]} \cos \phi_1(t)$ $\beta_2(t) = \sqrt{\frac{1}{2} [1 + a \operatorname{sn}(u, k)]} \sin \phi_0(t)$ $\beta_3(t) = \sqrt{\frac{1}{2} [1 - a \operatorname{sn}(u, k)]} \sin \phi_1(t)$ <p>$\{a, \gamma_0, \gamma_1, \gamma_2, \gamma_3\}$ are constants defined by initial conditions and inertias.</p>
	<p>and</p> <p>$\phi_0(t)$ and $\phi_1(t)$ are functions involving incomplete elliptic integrals of the third kind.</p>

The body-fixed components of angular velocity are denoted by ω_1 , ω_2 , and ω_3 and these are functions of the time t and constants defined in terms of principal moments of inertia and initial conditions. The Jacobian elliptic functions $\text{dn}(u, k)$, $\text{sn}(u, k)$, and $\text{cn}(u, k)$ are the basic time functions involved in the solutions for ω_1 , ω_2 , and ω_3 .

For the attitude description, Euler orientation parameters were chosen. The body's inertial attitude is defined by the α_j , $j = 0, 1, 2, 3$, which are expressible as functions of a set of four constant Euler parameters γ_j , $j = 0, 1, 2, 3$, (which define the orientation of a nonrotating angular momentum coordinate frame), and four time varying Euler parameters β_j , $j = 0, 1, 2, 3$, (which define the orientation of the principal axes of the body relative to the angular momentum frame). The β_j may be expressed as functions of time by using Jacobian elliptic functions, incomplete elliptic integrals of the third kind and, of course, initial conditions and inertias.

Transition trajectories may, in principle, be defined in terms of any set of attitude variables. Two particular four parameter sets were chosen. The Euler parameters α_j , $j = 0, 1, 2, 3$, are a rather obvious choice; however, preliminary studies have indicated that the set composed of the principal angle of rotation ϕ and the direction cosines ℓ_j , $j = 1, 2, 3$, of the Euler axis may be a more desirable set. These will be referred to as the principal rotation parameters. The construction of transition trajectories using these two sets of variables is summarized in the following list.

Definition of Transition Trajectories

Principal Rotation Coordinates

$(\alpha_0, \alpha_1, \alpha_2, \alpha_3) \Rightarrow (\phi, \ell_1, \ell_2, \ell_3)$ Transformation

$$\left. \begin{aligned} \phi_f(t) &= 2\cos^{-1}(\alpha_{f_0}) \\ \ell_{f_i}(t) &= \alpha_{f_i} / \sin \frac{\phi_f}{2} \end{aligned} \right\} f \rightarrow b$$

Forward Trajectory

$$\phi_f(t) = \text{Function (inertias, actual initial state at } t_0, t)$$

$$\ell_{f_i}(t) = \text{Function (inertias, actual initial state at } t_0, t) \quad i = 1, 2, 3$$

Backward Trajectory

$$\phi_b(t) = \text{Function (inertias, desired final state at } t_f, t)$$

$$\ell_{b_i}(t) = \text{Function (inertias, desired final state at } t_f, t) \quad i = 1, 2, 3$$

Transition Trajectory

$$\phi(t) = w_f(\tau)\phi_f(t) + w_b(\tau)\phi_b(t)$$

$$\ell_i(t) = w_f(\tau)\ell_{f_i}(t) + w_b(\tau)\ell_{b_i}(t) \quad i = 2, 3$$

$$\ell_1(t) = \pm \sqrt{1 - [\ell_2^2(t) + \ell_3^2(t)]}$$

Euler Parameters

Forward Trajectory

$$\{\alpha_f(t)\} = \text{Function (inertias, actual initial state at } t_0, t)$$

Backward Trajectory

$$\{\alpha_b(t)\} = \text{Function (inertias, desired final state at } t_f, t)$$

Transition Trajectory

$$\alpha_i(t) = w_f(\tau)\alpha_{f_i}(t) + w_b(\tau)\alpha_{b_i}(t) \quad i = 1, 2, 3$$

$$\alpha_0(t) = \pm\sqrt{1 - [\alpha_1^2(t) + \alpha_2^2(t) + \alpha_3^2(t)]}$$

Note that when four parameters are used appropriate constraints must be introduced.

The transition trajectory concept has been used to generate transition trajectories and the associated torque time histories for several pairs of initial and final states. Figures 9 and 10 show results for a case in which the principal rotation parameters were used to generate the transition trajectory. The principal moments of inertia picked for the example are $I_1 = 3$, $I_2 = 2$, and $I_3 = 1$. The maneuver required was to change the rotational state of the spacecraft from one in which $\alpha_0 = \sqrt{3}/2$, $\alpha_1 = \sqrt{15}/8$, $\alpha_2 = 1/8$, $\alpha_3 = 0$, $\omega_1 = 1$, $\omega_2 = 0.10$ and $\omega_3 = 0.0$ at $t = t_0 = 0$ to one in which $\alpha_0 = 1/4$, $\alpha_1 = \sqrt{15}/4$, $\alpha_2 = \alpha_3 = 0$, $\omega_1 = 0.101$, $\omega_2 = 0.0$ and $\omega_3 = 0.0$ at $t = t_f = 5.0$. In this maneuver the inertial components of angular momentum were changed from (2.93, 0.47, -0.48) at $t = 0$ to (0.303, 0.0, 0.0) at $t = 5$. Basically, a state in which the spacecraft is rotating rapidly with an initial nutation angle of about 12° is changed by the maneuver into a state of much slower (an order of magnitude less) spin about the principal axis of maximum moment of inertia, with the orientation of the body's angular momentum vector also changed.

The time histories of the angular momentum components and the Euler parameters are presented in figure 9. The principal rotation parameters were averaged to produce the transition maneuver, but the angular velocity and Euler parameters are, of course, also averaged in the sense that the desired final state is reached in a smooth manner. On each plot in figure 9, the solid curve represents the time history of the indicated variable which results from unforced forward integration, the dashed line has a similar interpretation, but is derived from the backward integration of the desired final state, and the bold curve is the transition curve. Very smooth transitions of all seven variables are evident.

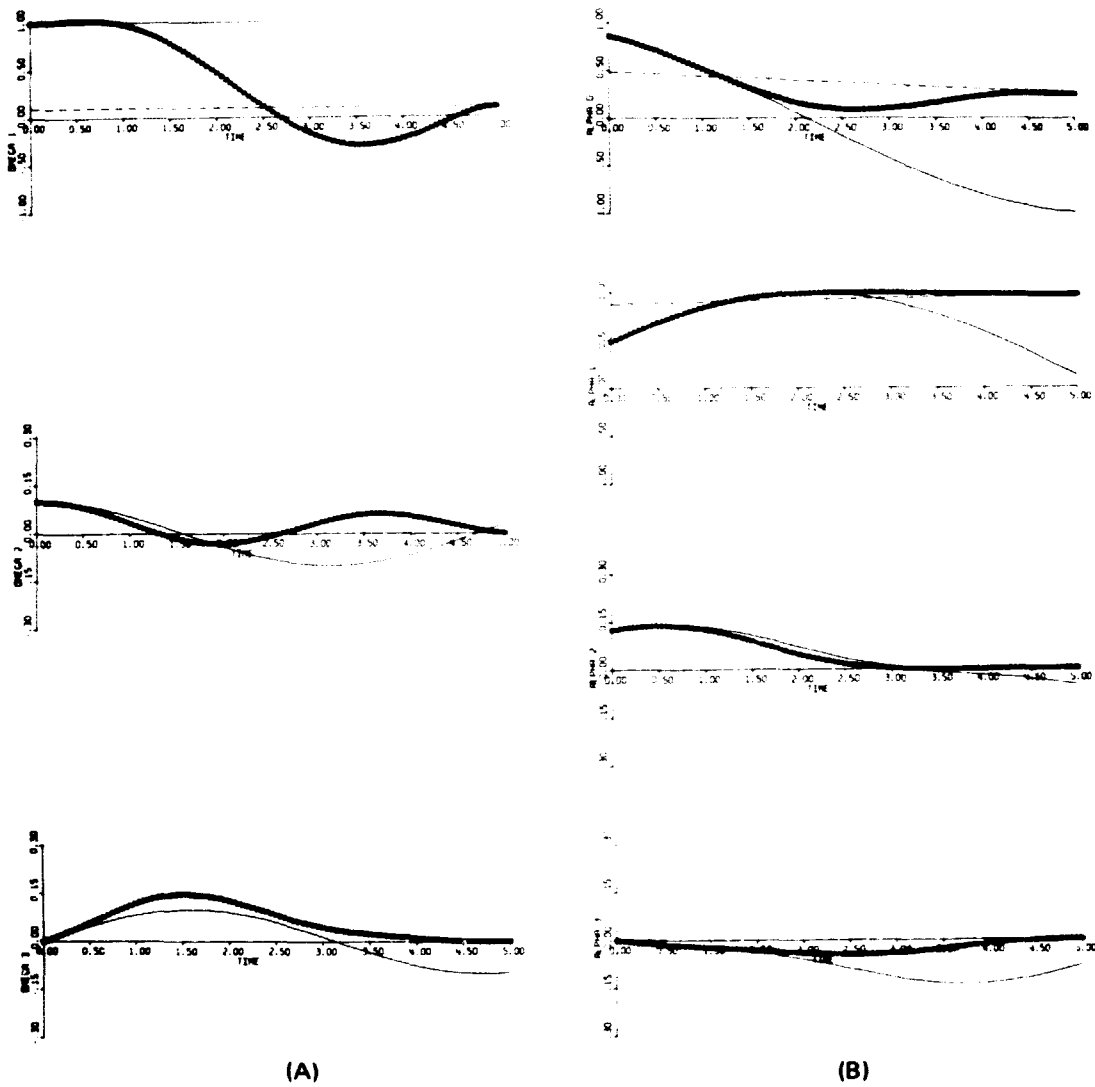


Figure 9. A - Angular velocity; B - Euler parameters.

Time histories for the variables which were averaged (i.e., the principal rotation parameters) are shown in figure 10. Also in figure 10 are included the time histories of the body-fixed components of the torque needed to generate the transition maneuver. The three curves in each of the plots indicated as LHAT1, LHAT2, LHAT3, and PHI are analogous to those previously described. In the torque plot, the 1-component is indicated by the solid line, the

2-component by the dashed line, and the 3-component by the bold line. The difference in the magnitudes of the initial and final angular velocities is apparent from the radically different slopes of the curves for the forward and backward solutions for the principal angle.

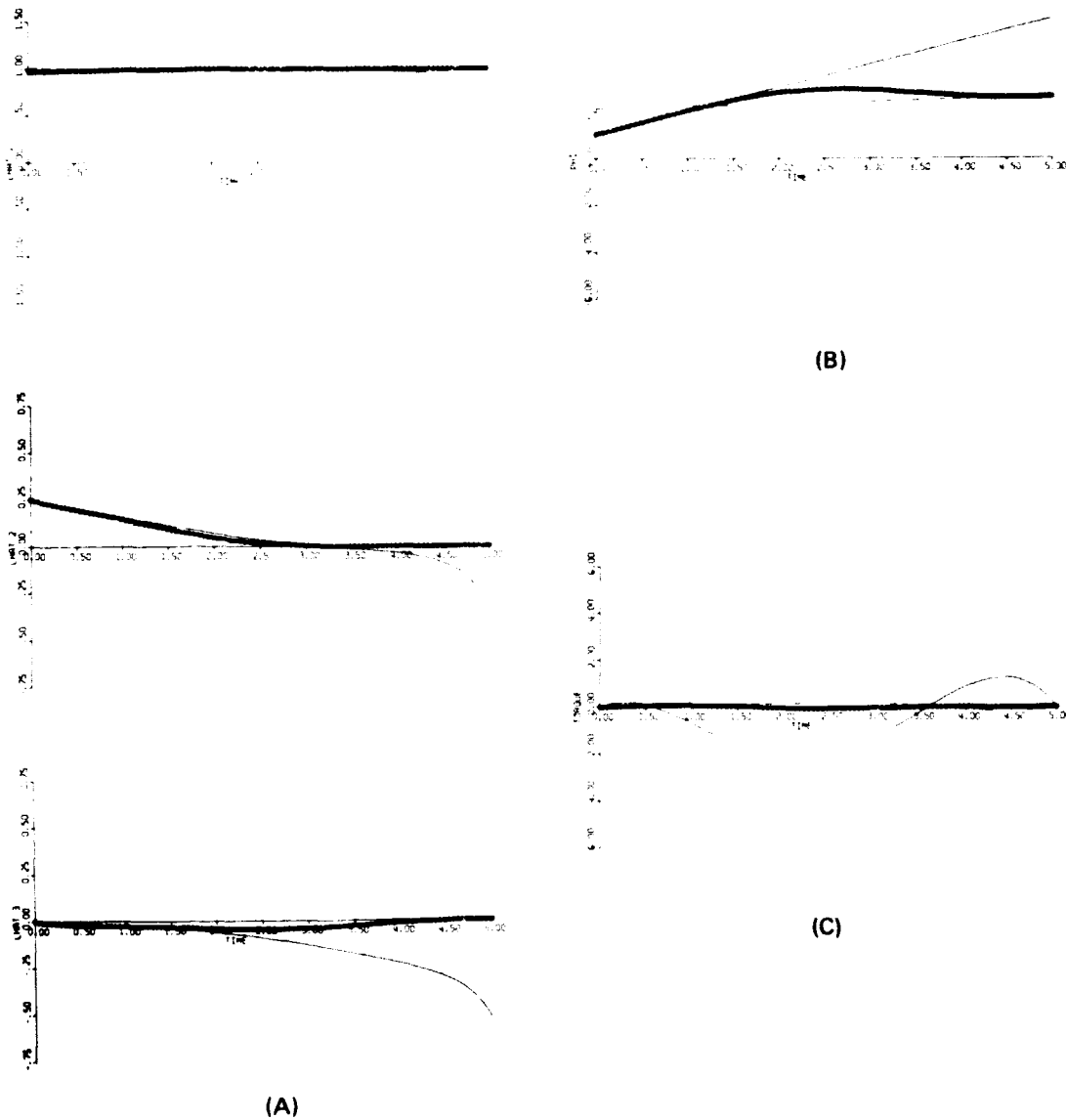


Figure 10. A - Euler axis direction cosines; B - principal angle; C - torque history.

Considering the torque history in more detail, we note that the second-order osculation constraints embodied in the functions W_f and W_b result in zero torque at $t = 0$ and $t = 5$. All three components of the torque are smooth and bounded; the largest magnitude of any one component is about 2.15.

Referring to the list of transition trajectories, the transformation from the Euler parameters to principal rotation parameters embodies a singularity whenever ϕ is an integer multiple of 2π ; resulting in ambiguous definition of the Euler axis. Thus, in the absence of some remedial action, the transformation equations and their derivatives do not provide an acceptable basis for defining multirevolution transition maneuvers. We are currently studying means of circumventing this difficulty and thereby allowing application of this method to the multirevolution case.

From the work which we have done to date on the attitude maneuver problem, we have drawn the following conclusions:

- Single-axis maneuvers are not necessarily optimal, but provide a reasonable basis for quiescent-state-to-quiescent-state attitude maneuvers using onboard computations and continuous torques, especially if the spacecraft is asymmetric.
- Control of such single-axis maneuvers in the presence of disturbances is feasible.
- Transition maneuvers provide an explicit solution to a more general class of maneuver problems.
- Control of transition maneuvers looks feasible.
- An important feature of both methods is that iterative solution of a two-point boundary value problem (TPBVP) is avoided.
- Transition maneuvers provide starting solutions (which satisfy the boundary conditions) for iterative solution of TPBVPs.

REFERENCES

- Crisp, R., D. Keene, and M. Dixon, 1967, "A Method of Spacecraft Control," *International Astronautical Federation, 17th International Astronautical Congress*, Gordon and Beach, New York.
- Cochran, J. E., B. K. Colburn, and N. D. Speakman, "Adaptive Spacecraft Attitude Control Utilizing Eigenaxis Rotations," AIAA Paper No. 75-158, AIAA 13th Aerospace Sciences Meeting, Pasadena, California.
- Dixon, M. V., T. N. Edelbaum, J. E. Potter, and W. E. Vandervelde, 1970, "Fuel Optimal Reorientation of Axisymmetric Spacecraft," *Journal of Spacecraft*, 7, pp. 1345-1351.
- Jancaitis, J. R., and J. L. Junkins, 1974, "Modeling in n Dimensions Using a Weighting Function Approach," *J. of Geophys. Res.*, 79, pp. 3361-3366.
- Kraige, L. G., and J. L. Junkins, 1974, "Perturbation Formulations for Satellite Attitude Dynamics," AIAA Paper No. 74-785, AIAA Mechanics and Control of Flight Conference, Anaheim, California.

Meyer, D., 1966, "On the Use of Euler's Theorem on Rotations for the Synthesis of Attitude Control Systems," NASA TN D-3643.

Morton, H. J., Jr., J. L. Junkins, and J. N. Blanton, "Analytical Solutions for Euler Parameters," *Celestial Mechanics*, in press; also 1973, AIAA/AAS Astrodynamics Conference paper, Vail, Colorado.

**MISSION OPERATIONS FOR THE LOW COST
MODULAR SPACECRAFT**

R. L. des Jardins
Goddard Space Flight Center
Greenbelt, Maryland

The low cost modular spacecraft (LCMS) was developed by Goddard Space Flight Center to provide a standard spacecraft bus which could easily be configured to support virtually any near-space unmanned mission to be flown in the 1980s. The LCMS features subsystem modularity allowing great flexibility and on-orbit servicing, yet achieving benefits of widespread standardization. Also, the LCMS design incorporates a high-performance onboard computer as a remote controller for most spacecraft subsystems. The LCMS is described briefly and its implications for mission operations is explored.

ONBOARD ORBIT DETERMINATION USING SERIES SOLUTIONS

T. Feagin

*University of Tennessee Space Institute
Tullahoma, Tennessee*

An iterative, linear sequential estimation algorithm is presented which is suitable for use in a small onboard digital computer. The solution is obtained in the form of a finite series of Chebyshev polynomials. The series-solution provides a close approximation to the actual orbit which is valid for a given interval of time. A Kalman filter is used to combine new observational data with the old estimate of the state and its associated error covariance matrix in order to update the series-solution and thus to provide a new optimal estimate and covariance matrix.

HIGH ALTITUDE AUTONOMOUS NAVIGATION

Howard A. Garcia
Martin Marietta Corporation
Denver, Colorado

PURPOSE OF STUDY

The applied research described in this paper pertains to a high altitude autonomous navigation system which was the subject of a Phase 0 Preliminary Design and Feasibility Study under contract with SAMSO, United States Air Force Systems Command. This contract had the expressed objectives of selecting a particular design configuration by means of a trade study involving several candidate sextant concepts and carrying out a preliminary design based on the final selected sextant subsystem. In addition, the contract also called for an analytic evaluation of the general navigation concept by a numerical analysis which included a parametric sensitivity study and a performance demonstration by a Monte Carlo analysis.

SYSTEM REQUIREMENTS

Air Force requirements specified that the system be autonomous to the extent that no dedicated earth emission would be necessarily invoked and that the system would operate effectively to at least 120,000 n.m. The space sextant system that was adopted relies upon no earth referenced missions, either passive or dedicated. The navigation accuracy has been shown to be constant for any of the tested orbits, irrespective of orbit shape, orientation, or altitude. The Air Force requirements further specified that the system should have a demonstrated accuracy (by numerical analysis) of at least 1 n.m. (1 σ rss) at a confidence level of 95 percent and, where large trajectory errors are presumed to exist, should converge in at least 10 hours from the onset of navigation. The numerical analysis has shown that the system converges to less than 1 n.m. in about 6 minutes and has demonstrated steady-state navigation accuracies of about 800 feet (1 σ rss) after 15 to 18 hours of measurement processing. Other design goals established for the system include mission versatility, satellite versatility, insensitivity to reasonable parameter variations, insensitivity to satellite maneuvers, a 5-year lifetime, and the utilization of existing technologies.

NAVIGATION CONCEPT

The navigation concept is simple and direct. Navigation is accomplished by means of measured angles between the brighter stars (visual magnitude < 2) and the bright limb of the moon. Reduction to the moon's center, including compensation for asphericity effects

and lunar terrain, is accomplished by onboard software. The essential data required to determine the navigation position are the measured angle, the moon's ephemeris, and precise time. In principle, it may be shown that angular measurements from each of two stars to its nearest limb on the moon establishes a line of position for the spacecraft. Similar measurements made on the earth's limb provide a second line of position. The intersection of the two obtains a complete navigation fix in as short a period of time as is necessary to complete these measurements.

High navigation accuracy is achieved by further improving this position (and velocity) knowledge by recursively filtering subsequent star-moon measurements over the next several hours.

ANGLE MEASUREMENT SUBSYSTEM

The basic sextant instrument consists of two Cassegrainian telescopes, an angle measurement head, and two gimbals providing for two additional degrees of angular freedom.

The electronics package consists of an oscillator, registers, A to D converters, a digital microprocessor, and the wheel speed control servo. The total device, sextant and electronics, would weigh less than 25 pounds.

The principle of operation is quite simple. A spinning element inside of the measurement head, running at constant angular velocity, intercepts the optical path of a ray originating at a star observed by one telescope, and subsequently intercepts the path of a ray originating on the moon's limb observed by the second telescope. The time elapsed between the reception of these two signals, which may be recorded with great precision, is directly translatable into arc measure. This associated servo system incorporates two independently operated subsystems: an in-plane servo which positions the star (S) and the limb (L) trackers precisely on these respective targets and a cross-plane servo which orients the measurement head (wheel and both optical tracking telescopes) into the plane of measurement defined by the $S \times L$ vector.

MEASURING HEAD OPTICAL SCHEMATIC

Two optical trains are utilized in the operation of each tracker: the tracker ray and the timing pulse ray. The tracking ray enters the telescope aperture, reflects off the primary mirror, then the secondary mirror, and finally impinges on the detector. The timing pulse ray, originating at an internal light source, passes through the collimator lens and is reflected off two mirrored surfaces in a prism that is common to both trackers and that rotates with the wheel. This timing pulse ray is then reflected off this primary and secondary and impinges on the same detector as the tracking ray. The detectors are two-stage, four quadrant, differential detection types, with the first stage for acquisition and the second stage for precise tracking the timing pulse generation. The timing pulse is generated by zero crossing detection of the timing pulse ray as it crosses two detectors whose output is differenced. One advantage of this type of detection is the accuracy that can be

achieved with zero crossing detectors and another is its insensitivity to a mismatch in detector output responsiveness.

The sextant trackers are designed for total symmetry and reciprocity so that either tracker can be used for star or limb tracking. This feature also allows for attitude measurement and onboard self-calibration using two stars.

SYSTEMATIC ERROR COMPENSATION

High measurement precision and stability is achieved by means of a phase-locked loop and self-compensation for radial runout and encoder disk systematic errors. The phase locked loop drives the wheel assembly at an angular velocity of approximately 50 rad/s. The commanded rate originates with the oscillator and the position feedback is derived from an optical transducer disk by means of a read head. When the wheel is in motion, the output from the read head is frequency. The actual disk contains inscribed $\sin 2^{11}$ and $\cos 2^{11}$ functions. These functions permit the extraction of phase information and make a wideband, high gain phase loop possible.

Systematic errors in the encoder disk are on the order of 10 arc-seconds until self-compensation procedures are activated. Other error sources which include bearing noise, sensor noise, and data sampling become dominant after self-compensation; however, the combined effect is to yield a total measurement error of about 0.5 arc second over a one second measurement time interval. The automatic tracking provision allows for continuous measurements during low thrust maneuvers. During high acceleration maneuvers, however, the sextant will be caged, but may resume operation within one minute following the maneuver.

NAVIGATION PERFORMANCE

The principal outcome of the analytic investigation of the system performance was to demonstrate that the system is capable of exceeding Air Force requirements by a substantial margin, both with regard to navigation accuracy as well as convergence time. A Monte Carlo simulation consisting of 59 samples (with no outliers) was necessary to ensure a 95 percent confidence level in the order statistics, constituting the primary investigative tool used in the performance analysis.

Two orbits were used as the models for the Monte Carlo analysis. Orbit A is a highly eccentric, 12-hour Molnyia type orbit, and Orbit B is an equatorial, circular, geosynchronous orbit. The Monte Carlo analysis considered only star/lunar limb measurements; consequently, these results show the high dependence of convergence time upon orbit geometry, for instance, 7 hours for Orbit A and 12 hours for Orbit B. By definition, convergence time is the time from the onset of navigation to the last major inflection of the navigation error curve; however, system accuracy continues to improve with additional data processing so that ultimate steady-state accuracy is finally achieved after several days of sextant navigation where the moon has completed a significant segment of its orbit. The accuracy is on the order of 800 feet and is a reflection primarily of the uncertainty in the lunar ephemeris itself.

A later analysis which employed star/earth limb measurements to augment the star/lunar limb measurements showed that the convergence time could be reduced to a few minutes. The final system accuracy would be achieved in less than 20 hours, owing to the vastly improved geometry resulting from the intersection of the second line of position. In either case, the ultimate navigation accuracy depends upon the more precise lunar limb data which is the primary mode of navigation, the earth limb data being used only to speed up convergence and to supplement the lunar limb data when the moon is occulted by either the earth or the sun.

STATISTICAL AGREEMENT

The performance analysis used several statistical methodologies to represent the expected system accuracy, all of which demonstrated good relative agreement, indicative of a fundamental internal consistency and providing a firm basis for the main conclusions drawn from the study. Four curves, all representative of the 1σ case, were computed and plotted for the two demonstration orbits:

- 67% - 67% population coverage derived from histogram data across 59 samples;
- σ - ensemble statistics standard deviation across 59 samples;
- σ_{cov} - square root of the summed position eigenvalues from a covariance analysis; and
- σ_3 - square root of the second central moment derived by a time averaged (moving window) technique along a single sample simulation.

An apparent disagreement between the covariance analysis and the Monte Carlo results at the initial time was due to the methods used to initialize the respective trajectory errors. The initial state covariance for these orbits was set at the estimated 1σ values; whereas, the initial trajectory offset for simulation purposes was set at 3σ values for all six state elements (a probability of occurrence of only $7 \cdot 10^{-20}$). Furthermore, the σ_3 curve, being one sample from the Monte Carlo set, is also shown to deviate initially from the other curves. The important result, however, is the fact that all of the statistical methods converge to essentially the same values at steady state for each of the two performance test cases, Orbits A and B.

SENSITIVITY ANALYSIS

A sensitivity analysis was carried out on three high altitude orbits (Orbit C, 14,350 n.m.; Orbit D, 68,000 n.m.; Orbit E, 115,000 n.m.) in addition to Orbits A and B. First and foremost, these sensitivity analyses have demonstrated that the system is totally indifferent to altitude in the earth-moon domain. Of course, this result is not unexpected because the prime observable is the moon and not landmarks on the earth. In the absence of augmented observations using the earth's limb, the rate of convergence appears to obey a logarithmic function based on orbit period. However by exploiting earth limb measurements,

all orbits converge in the period of a few minutes and obtain steady-state navigation accuracies of less than 0.2 n.m. in a matter of hours.

The sensitivity analysis also considered a range of model parameter errors of up to twice nominal values. These parameters included the lunar ephemeris ($1 \sigma = 600$ feet), lunar terrain height, ($1 \sigma = 1700$ feet), sensor noise ($1 \sigma = 0.566$ arc sec), and initial trajectory errors, the latter being dependent upon the particular orbit type. The principal results were as follows:

- The system is virtually insensitive to expected lunar ephemeris errors, even for the twice nominal case;
- $2 \times$ lunar terrain errors are acceptable, but this also means that onboard compensation for terrain height will be required;
- Nominal sensor errors are near optimal in view of the contribution of other modeled system errors; and
- Large dispersions in initialization errors were completely suppressed by the recursive filtering process.

OCCULTATION OF THE MOON BY THE EARTH OR SUN

A phenomenon that must be acknowledged by the system concerns the possibility of an occultation of the moon by either the earth or the sun. The effect upon the navigation system was investigated by simulation, and it was found that the navigation accuracy was largely unaffected so long as the augmented measurement mode (earth limb) was employed during these critical periods.

In the specific example tested, worst case geometry was assumed for Orbit B (24-hour, circular orbit), where the earth itself is twice occulted by the sun in 24 hours, and the moon is concurrently obscured by the sun for 30 hours. Prior to either of the occultations in this example, the large initial trajectory errors were reduced by combined earth limb and lunar limb measurements. The earth and moon were then presumed to enter simultaneously the 9° look angle constraint zone centered about the sun. No navigation data could be acquired until the earth was again visible after 1.5 hours, and a slight increase in navigation error may be noted. Earth measurements were then commenced for the next 22.5 hours when it was again occulted; however, the growth of navigation errors this time were sufficiently suppressed so that no noticeable increase in navigation error occurs during the second occultation. Lunar limb measurements were resumed after 30 hours.

PRECISION ATTITUDE REFERENCE SYSTEM

The principal feature of the Space Sextant Navigation System is the high precision of the angular measurement. This same feature conduces to make the device an attitude reference sensor as well. The latter capability shows promise of becoming one of the most accurate onboard attitude sensing systems in existence. As an attitude sensor, it will be

necessary to add a platform reference mirror and a precision three axes gyro package. An autocollimation light source would also be added to the basic instrument in order to permit one telescope at a time to align itself with the reference mirror. Two axis angular reference may be achieved either with a second orthogonal reference mirror or a precision base encoder to measure the yaw angle. The relative advantages of these two alternative modes of obtaining two angular measurements of a single star have not been assessed at this time; however, it is anticipated that the system will ultimately be capable of 0.1 arc sec, three axes orientation under steady-state conditions.

SS-HANS DESIGN SUMMARY AND CONCLUSIONS

A fundamental included angle accuracy of 0.5 arc sec (1σ) by the Space Sextant makes navigation practical in cislunar space to a high degree at accuracy (< 0.2 n.m.) and at the same time provide the highest level of autonomy possible. An attitude reference system of 0.1 arc sec precision is also feasible, employing the basic sextant instrument modified to perform autocollimation in conjunction with a fixed mirror system. The sextant and its associated electronics will weigh less than 25 pounds and will require 7.5 watts average power, 50 watts peak power, and 30 watts during actual measurement. Design lifetime is 5 years with redundancy and parts derating, bearings included.

The Space Sextant is designed to be functionally subservient to the spacecraft computer system and to impose no cycle time restrictions on the computer. Software functions including navigation, on-orbit calibration and health monitoring will require 15K of 16 bit words of memory. Read-only mass storage for a 5-year lunar ephemeris and lunar terrain height data will require up to 140K of 30 bit words. The latter needs may be fulfilled either by a solid-state ROM of less than 4 pounds or by magnetic tape units. The read-only provision greatly enhances the long life and reliability of either type of mass storage device.